Bull. Chem. Soc. Ethiop. **2025**, 39(2), 257-270.
DOI: https://dx.doi.org/10.4314/bcse.v39i2.6

ISSN 1011-3924
Printed in Ethiopia
Online ISSN 1726-801X

SYNTHESIS AND SPECTROSCOPIC CHARACTERIZATIONS OF ZINC(II) OXIDE IN NANOSIZED RANGE AS A SMART MATERIALS IN TREATMENT AND RECYCLING OF WASTEWATER

Mohamed Y. El-Sayed[1*], Yasser A. El-Ossaily[1], I.M. Ahmed[1], Tamer H.A. Hasanin[1], Q. Mohsen[2] and Moamen S. Refat[2]

[1]Department of Chemistry, College of Science, Jouf University, Sakaka 2014, Saudi Arabia
[2]Department of Chemistry, College of Science, Taif University, P.O. Box 11099, Taif 21944, Saudi Arabia

(Received August 21, 2024; Revised November 8, 2024; Accepted November 12, 2024)

ABSTRACT. The new reaction between zinc(II) chloride and glutaconic acid ($C_5H_6O_4$) was studied. The results indicate the formation of zinc(II) glutaconate complex with a molar ratio of metal to organic ligand (glutaconic acid) of 2:1 with the general formula $[Zn_2(C_5H_4O_4)(Cl)_2(H_2O)_2].4H_2O$. The infrared spectrum of the glutaconate suggested that the two carboxylate groups are bidentate chelating. The current study uses a thermal breakdown approach to synthesize zinc oxide (ZnO) nanoparticles (NPs). The synthesized ZnO NPs were characterized using X-ray diffraction (XRD), scanning electron microscope (SEM), energy dispersive X-ray analysis (EDAX), and Fourier transform infrared spectroscope (FTIR). The crystallite size was calculated using Scherer's formula, which was 54 nm. The degradation of hydrogen peroxide, or H_2O_2, solution was used to test the produced ZnO NPs' catalytic activity performance. The results showed that ZnO NPs could efficiently break down H_2O_2. The ZnO NPs' photocatalytic capabilities have been assessed using methylene blue (MB) and UV light in an aqueous solution, according to the data, 77% of photocatalytic degradation towards MB in 240 min occurs.

KEY WORDS: ZnO NPs, Methylene blue dye, Photocatalytic, Metal-glutaconate complexation.

INTRODUCTION

Metal oxides are an important family of materials used in environmental research, biology, electrochemistry, chemical sensors, catalysts, magnetism, and other domains [1-4]. There are numerous uses for transition metal oxide nanoparticles, including as adsorbents [1], superconductors [2], sensors [3], and catalysts [4]. Hydrothermal [5], sol-gel [6], combustion [7], precipitation-gelation, gel citrate [8], mechanochemical process [9], urea-assisted homogeneous precipitation [10], gas condensation [11], and microwave plasma are some of the methods developed for the synthesis of metal oxide nanoparticles [12]. Given that nanoparticles act as sensors and probes for the delivery of biomolecules into cellular systems, nanobiotechnology is the branch of nanotechnology that develops and applies nanotechnology instruments to research biological phenomena. A further area of study in nanobiotechnology is the environmentally benign synthesis of biogenic, biocompatible, and reasonably priced nanomaterials [13]. Nanomaterials can be used for a wide range of purposes, including catalytic membranes, nanosorbents, bioactive nanoparticles, and metal nanoparticles including titanium oxides, iron, and silver [14,15]. The most significant and necessary element on earth is water, however, human activity is constantly lowering the quality of water supplies. Water and wastewater treatment are two areas where zinc oxide is often used. ZnO is widely used in self-cleaning, environmental purification, and photocatalysis, among other processes. The development of nanotechnology has enhanced ZnO activity and considerably influenced photocatalysis [16, 17].

*Corresponding authors. E-mail: myelsayed@ju.edu.sa

With so many uses, from the relevance of metal-carboxylate complexes as model systems for the metalloactive sites in bioinorganic chemistry [18, 19] to their utility as novel materials in materials science, the chemistry of metal-carboxylates is still being thoroughly investigated. Thermal decomposition techniques can be used to easily create metal oxides from metal-carboxylate precursors [20]. Interesting structural properties are exhibited by metal-carboxylates. Because the carboxylate group exhibits versatile ligation behavior, it can function as a monodentate ligand, a bridging bidentate ligand coordinating with two metals, or a bidentate ligand binding to a single metal, accounting for the structure diversity observed in metal-carboxylate complexes [21-23]. Attached to the fully saturated glutaric acid, glutaconic acid is a member of the class of substances called dicarboxylic acids and derivatives.

There have been thousands of recorded cases of biological, inorganic, and organic pollutants in water [24]. A number of them are poisonous and have major adverse effects; some are even deadly and cancerous. These pollutants pose a serious risk to human health, aquatic life, and the earth's ecology overall [25]. Dyes are among the many substances that make up industrial wastewater and are regarded as significant pollutants. Dyes' great thermal and photostability allow them to linger in the environment for a long time. Numerous colors are poisonous to life, mutagenic, and carcinogenic, as are the breakdown products of these dyes. They are usually not eliminated from water by wastewater treatment systems and traditional methods including adsorption, ultrafiltration, chemicals, and electrochemical processes as they are not easily biodegradable [26-28]. The availability of clean water is now a constant problem for humanity [29] because water contamination poses a serious threat to aquatic habitats and social health [30]. The industries that engineer dye wastewater mostly include textile, pulp, paper, paint, pharmaceutical, cosmetics, and food [31]. The growing problem of waterbody contamination has made it difficult for aquatic animals to live and consume [32,33]. This is because untreated wastewater or effluent is discharged into the water body, making the inhabitants toxic to them and their surroundings [33].

It has been shown that photocatalysis is a viable technique for treating wastewater that contains both organic and inorganic contaminants. Many academics have been interested in this method in recent years to remove pollutants from water, like pesticides and dyes [34]. A number of these studies have employed semiconductor aqueous solutions irradiated by UV light to analyze contaminants through photodegradation. Water contamination, both surface and ground, has increased in recent years because of population growth. Owing to their high toxicity and lack of biodegradability, organic dyes used in the food and textile sectors are thought to be the primary sources of environmental pollution and harm human health by causing cancer. Methylene blue (MB) dye is used in a few industries, including cotton, jute, paper, wool, leather, and silk [35]. It is also added to food coloring. Methylene blue dyes have significant impacts on the immune system and reproductive system. They also show genotoxic effects and may be carcinogenic [36]. Therefore, these dangerous colors need to be removed from industrial effluents. Many techniques have been employed, including biological treatment [37], adsorption [38], and photocatalysis [39, 40], to remove these colors from industrial effluents. The use of photocatalysts in water and air pollution has been shown to reduce the harm that organic dye pollution causes to people and the environment by either breaking down hazardous organic compounds or converting them into less harmful molecules [39]. Consequently, the field of study on photocatalysis employing heterogeneous catalysts is intriguing as this technique aids in the full mineralization of these environmentally dangerous dyes [40].

Here in the present study, nanostructured ZnO material was prepared via the controlled thermal decomposition in the air of the zinc(II) glutaconate complex, and this material was analyzed for its structural and morphological properties using the FTIR, XRD, SEM, TEM, and EDX techniques. The zinc(II) glutaconate complex which was used as precursor $[M_2(C_5H_4O_4)(Cl)_2(H_2O)_2].4H_2O$. The catalytic degradation of the prepared ZnO material as a

catalyst toward H_2O_2 was examined at room temperature as well as investigated the effectiveness of ZnO-NPs on the removal of methylene blue (MB) from aqueous solution.

EXPERIMENTAL

Chemicals

All of the studies distilled water came from Millipore, France's Milli-Q direct 8 purification system. Zinc(II) chloride (≥98%), $ZnCl_2$, and glutaconic acid (97%) were bought from (Sigma-Aldrich). NH_4OH (30-33% NH_3 in H_2O), diethyl ether (≥98%), methanol (99%), and dimethyl sulfoxide (99%) were received from Aldrich-Sigma chemical company, St. Louis, Missouri, United States.

Synthesis of zinc(II) glutaconate complex

By combining stoichiometry quantities of zinc(II) chloride (2 mmol; 0.273 gm) with glutaconic acid (1 mmol; 0.131 g), the zinc(II) glutaconate complex was created. After neutralizing with ammonium hydroxide (1 M) in 25 mL methanol solution (1 mmol) of glutaconic acid, the mixture was gradually added to 25 mL (2 mmol) of $ZnCl_2$ in aqueous solution. Following ammonium hydroxide neutralization, the mixture was heated in a water bath for 2 h to a temperature of around 70 to 75 °C. The precipitate was filtered out, repeatedly rinsed in hot water to eliminate ammonium ions (NH_4^+), dried at around 80 °C to a consistent weight, and then placed in a vacuum over $CaCl_2$. The precipitate was then annealed in a muffle furnace for 2 h at 600 °C, and the ZnO NP were then produced.

Instrumentation

The molar conductance of the prepared 10 mol/cm^3 zinc(II) glutaconate complex in DMSO solution was measured by the HANNA Edge conductivity meter (Hanna Instruments, UK). The microanalytical analyses (% carbon, % hydrogen, and % nitrogen) contents was measured by using a Perkin Elmer CHN 2400, USA). The metal content was determined gravimetrically by converting the compounds into this corresponding oxide. FTIR spectroscope was used to characterize the new substance. First, a background spectrum was performed to provide a relative scale for transmittance strength, the yield spectrum in which the instruments attributes were disregarded, such that the spectra produced from samples contain just the spectral features of the samples. FT-IR spectra were considered molecular fingerprints of the material. Infrared spectra of zinc(II) glutaconate complex and zinc(II) oxide NPs were measured in the range of 400-4000 cm^{-1} on FT-IR Nicolet 6700, Thermo Scientific, USA. Thermogravimetric analysis was carried out in the temperature range of 25 to 700 °C in nitrogen atmosphere by thermogravimetric TGA–51analyzer, Shimadzu, Japan with heating rate 10 °C/min with platinum crucible. X-ray diffractometer (Bruker D8 Adv., Germany) with Ni-filtered Cu-Ka line as the radiation source (λ= 1.54056 Å) was used to create XRD patterns. X-ray diffractogram rang in 2θ = 10-80° at room temperature. Scanning electron microscope (SEM, JEOL.JSM-6610LV, Tokyo, Japan) was used to analyze the morphology of the surface employing a scan of a closely focused electron beam across the surface of the samples. Energy-dispersive X-ray detection was taken in JEOL.JSM-639OLA equipment with an accelerating voltage of 20 kV to study the chemical structure and composition of complexes. The transmission electron microscopy images were performed using JEOL JEM-1200 EX II, Japan at 60-70 kV.

Catalytic activity of ZnO NPs

By titrating the non-decomposed H_2O_2 with a standard $KMnO_4$ solution, ZnO materials' catalytic activity towards the breakdown of H_2O_2 was attained. In a conical flask, 100 mL of 0.1 N H_2O_2 and 100 mg of produced ZnO were combined at room temperature while magnetic stirring was in place. A range of time intervals, from 10 to 50 min, were used to evaluate the H_2O_2 breakdown. After that, a 5 mL aliquot of the reaction mixture was titrated in the presence of the acidic H_2SO_4 solution using 0.1 N of $KMnO_4$. The volume of the $KMnO_4$ solution was compared before and after the catalytic breakdown, and the difference was found.

Photocatalytic degradation of ZnO NPs

A conical flask was filled with a known amount of nano-synthesized zinc(II) oxide and 100 mL of an aqueous solution of methylene blue dye (MB) (10 ppm). Adsorption took place for 30 min, followed by 4 h of exposure (UV lamp). Absorbance was evaluated every 20 min by extracting 2 mL of the irradiated solution, centrifuging it for 15 min, and using a spectrophotometer to determine the filtrate's absorbance at its maximum wavelength (664 nm). The dye's decolorization rate was calculated and reported in Equation 1:

$$\text{Dye decolorization, } \% = (A_0 - A_t)/ A_0 \times 100 \quad (1)$$

where A_0 is each solution's starting absorbance and A_t is the absorbance at the specified time. Two variable factors were examined and their impacts on the photocatalytic degradation of the MB dye were the dose of nano-synthesized zinc(II) oxide and the length of irradiation.

RESULTS AND DISCUSSION

Zinc(II) glutaconate complex interpretation

For the characterization of a white solid zinc(II) glutaconate complex, $[Zn_2(C_5H_4O_4)(Cl)_2(H_2O)_2].4H_2O$ (Figure 1) was analyzed by elemental analyzer, conductivity, infrared spectroscopic, thermal analysis (TGA/DrTGA) and morphological characterization techniques like XRD, and SEM. The carbon, hydrogen, and chloride contents in the synthesized zinc(II) glutaconate were determined by elemental analysis, Mol. Wt.: 437.86, Yield: 86%, M.P. > 300 °C; Analysis calculated for $C_5H_{16}C_{l2}O_{10}Zn_2$: C, 13.72; H, 3.68; Cl, 16.19, Zn, 29.87% Found: C, 13.55; H, 3.60; Cl, 16.11; Zn, 29.79%; while content of zinc metal was determined from thermal gravimetric analysis by heating the prepared complex to most stable oxides at 800 °C. The content of crystallization water molecules was calculated from TGA curves and by heating the complexes at conforming temperatures. For zinc(II) glutaconate complex in dimethyl sulfoxide (DMSO) with 10^{-3} M concentration, the molar conductance value is Λ_m = 48 $\Omega^{-1}mol^{-1}cm^{-1}$, assigned to non-electrolytic nature [41]. This verified that outside of the coordination sphere, chloride ions were not present in ionic form.

FTIR analysis

The zinc(II) glutaconate metal complex was prepared as a solid with a molar ratio of metal to organic ligand of 2:1 with general formula $[Zn_2(C_5H_4O_4)(Cl)_2(H_2O)_2].4H_2O$. The prepared complex is characterized by FTIR spectra in Figure 2(A and B) and the assignments are presented in Table 1. When the acid is converted to the complexes, the bands of stretching vibration of the C=O group, υ(C=O) in the COOH group at 1697 cm^{-1} disappear, whereas the bands of asymmetric vibrations υas(OCO), at 1460 cm^{-1} and the bands of symmetric vibrations υs(OCO) at 1246 cm^{-1}

appears. In FTIR spectrum of the zinc(II) complex, there are broad absorption bands of υ(OH) with maximum at 3459 and 3352 cm^{-1} and characteristic bands of bending to water hydrated, $\delta(H_2O)$ at 163 cm^{-1} confirming the presence of crystallization water molecules linked by hydrogen bands, the bands of C-H vibrations at 1175, 1000-700 cm^{-1}. When compared to ionic form data (where the COO- groups' ($\Delta\upsilon = \upsilon as(OCO) - \upsilon s(OCO)$) values are smaller than the ionic salt value), the prepared complex difference between symmetrical and asymmetrical vibrations, as summarized in Table 1, strongly suggests that COO- groups are functioning as bidentate chelating ligands [42].

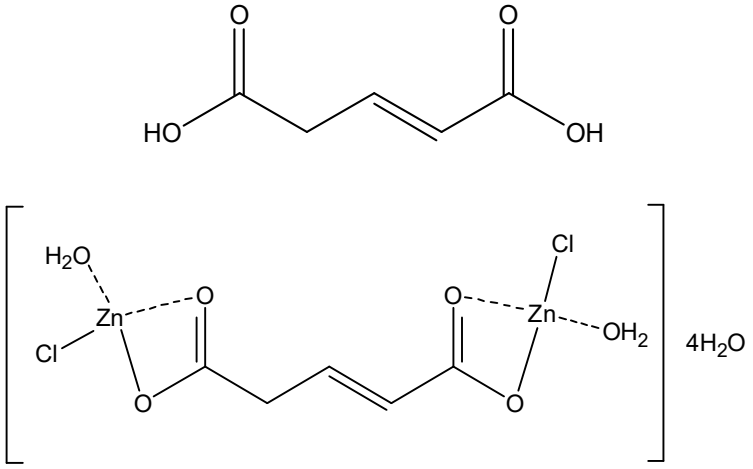

Figure 1. Chemical structures of glutaconic acid and $[Zn_2(C_5H_4O_4)(Cl)_2(H2O)2].4H_2O$ complex.

Table 1. Infrared frequencies (cm^{-1}) and tentative assignments for glutaconic acid (**A**), zinc(II) glutaconate complex (**B**), and zinc oxide NPs which were synthesized by annealing at 600 °C (C).

Compounds	Assignments						
	$\upsilon_{(O-H)}$	δ_{H2O}	$\upsilon_{(C=O);\ COOH}$	$\upsilon_{as\ (OCO)}$	$\upsilon_{s\ (OCO)}$	$\upsilon_{as} - \upsilon_{s}$	$\upsilon_{(M-O)}$
A	-	-	1697, 1655	-	-	-	-
B	3459, 3352	1630	-	1460	1246	214	523, 478
C	-	-		-	-	-	527, 443

Figure 2B displays the FTIR spectrum of the ZnO nanoparticles that were synthesized. The absorption peaks located at 527 and 443 cm^{-1} is indicative of the vibration mode of metal-oxygen (ZnO stretching vibrations). The functional group contained in the synthesized ZnO NPs is indicated by the peaks.

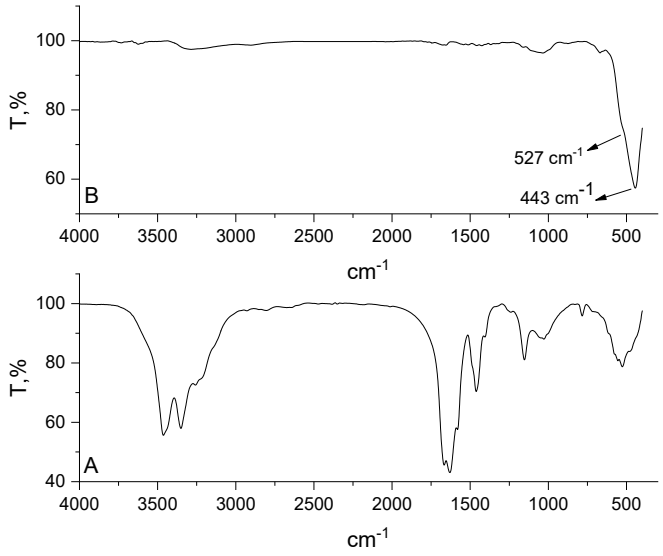

Figure 2. Infrared spectra of (A): zinc(II) glutaconate complex, and (B): zinc oxide NPs which are synthesized by annealed at 600 °C.

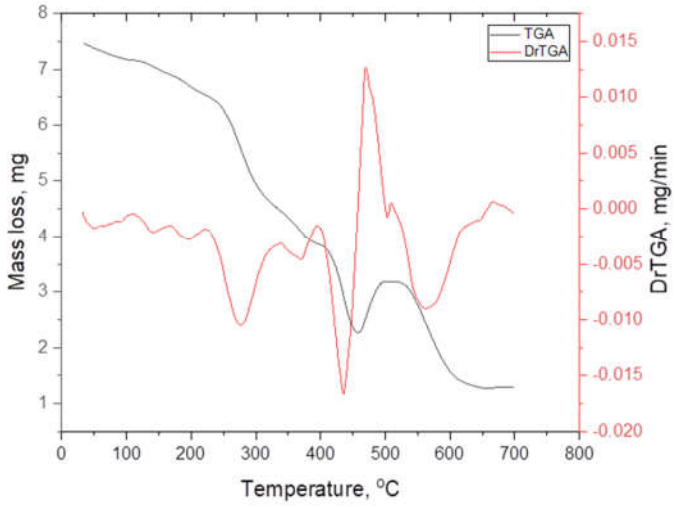

Figure 3. TGA/DrTGA of zinc(II) glutaconate complex.

Thermal analysis

The prepared zinc(II) complex is stable at room temperature. During heating, this is decomposed within temperature range 25-to-700 °C (Table 2, Figure 3). The hydrated zinc(II) glutaconate complex is stable up to 25-140 °C and on further heating, they are dehydrated in two stages started from 25-to150 °C and 150-to-250 °C, respectively to associated an anhydrous complex [1, 41]. After dehydration, the anhydrous compound decomposes in within 250-to-700 °C stage. The exothermic signal at 563 °C can be attributed to the decomposition reaction of the intermediate formed: $ZnCO_3$, with the loss of two coordinated water molecules, CO_2, chlorine gas, and two acetylene molecules with simultaneous formation of ZnO as a residual product.

Table 2. Maximum temperatures and mass loss values of the decomposition stages of $[Zn_2(C_5H_4O_4)(Cl)_2(H_2O)_2].4H_2O$ complex.

Decomposition stages	T_{max}/°C	Assignments	%weight losses	
			Found	Calc.
Stage, 25-150 °C	142 °C	$2H_2O$ (uncoordinated)	8.42%	8.22%
Stage, 150-250 °C	195 °C	$2H_2O$ (uncoordinated)	8.11%	8.22%
Stage, 250-300 °C	275 °C	$2H_2O$ (coordinated)	8.08%	8.22%
Stage, 300-650 °C	371, 435, 502, 563 °C	$Cl_2 + 2C_2H_2 + CO_2$	57.64%	58.03%
Total loss	25-to-700 °C	$6H_2O + Cl_2 + 2C_2H_2 + CO_2$	82.25%	82.69%
Residue	700 °C	ZnO	17.75%	17.31%

XRD analysis

In nature, zinc oxide appears as a crystalline material and exhibits n-type semiconductor characteristics. Its high excitation binding energy (60 meV), strong electrochemical coupling coefficient, low dielectric constant, outstanding optical absorbance, and wide band gap of 3.37 eV at room temperature [43]. The excellent purity of the ZnO synthesized utilizing the thermal decomposition in air of the zinc(II) glutaconate complex technique was confirmed by the observed ZnO spectrum. Figure 4 displays the X-ray diffraction of synthetic ZnO NPs. The X-ray diffraction map (Figure 4) reveals that ZnO is the sole substance or phase to exhibit peaks; this indicates that the sample synthesized is extremely pure. As can be observed in Figure 4, the sample's nanoparticle nature is reflected in the broadening of the X-ray diffraction lines. Several notable peaks in X-ray diffraction were taken into consideration, and the related d-values were compared to the standard [JCPDS file No. 80-0075] [44]. Metal oxide is pure zinc oxide with a hexagonal structure, as demonstrated by X-ray diffraction. The results of X-ray diffraction (XRD) showed that the diffraction peaks were located at 31.05°, 32.63°, 36.22°, 47.52°, and 56.61° with lattice planes of (100), (002), (101), (102), and (110), respectively. ZnO NPs' crystallite size was calculated using the Debye-Scherrer equation, and it was discovered to be 54 nm [45].

$$D = \frac{K\,\lambda}{\beta \cos\theta} \tag{2}$$

where the wavelength of the X-ray is λ and equal to (1.5418 Å) for Cu Kα radiation, K is taken as 0.94 and is constant, full width at half maximum (FWHM) is β of prominent intensity peak (100% relative intensity peak), and the peak position is θ.

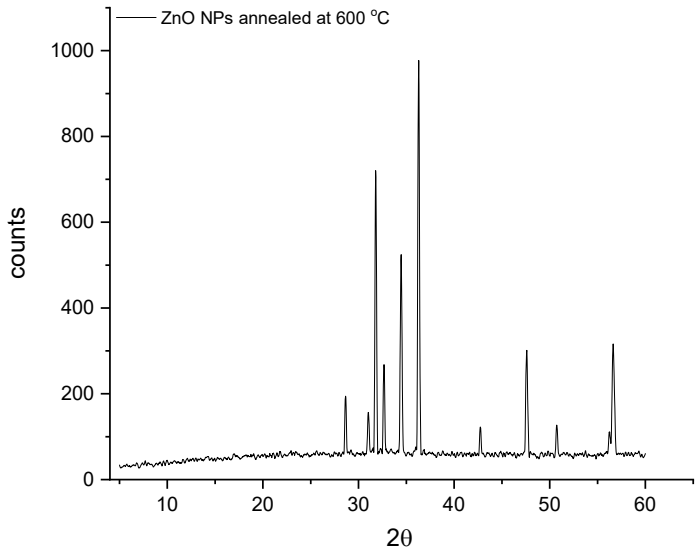

Figure 4. XRD patterns of ZnO NPs which were synthesized by annealed zinc(II) glutaconate complex at 600 °C.

SEM, EDX and TEM analyses

The SEM images of ZnO NPs (Figure 5A) made with the thermal decomposition in the air of the zinc(II) glutaconate complex approach showed the development of nanoparticles with considerable aggregation. ZnO nanoparticles were found to have precise structure. The capping agent (glutaconic acid) could be used to reduce particle size during synthesis. By measuring the intensity of the distinctively released X-rays, the energy dispersive X-rays Analysis (EDAX) tool was used to confirm the proportionate elemental composition of ZnO nanoparticles (Figure 6). Only the elements zinc and oxygen were detected by EDX in the synthesized ZnO NPs. The atomic and weight percent compositions of the elements (oxygen = 17.36%; zinc = 82.64%) are in agreement with EDX analysis verifying the synthesized ZnO NPs' purity [46]. TEM was used to evaluate the main particle sizes and morphologies of ZnO NPs produced using the annealed zinc(II) glutaconate complex at 600 °C. Most of the particles, have rods, grain-like shapes (Figure 5B), and are in the nanoscale range with the average size of 50 nm.

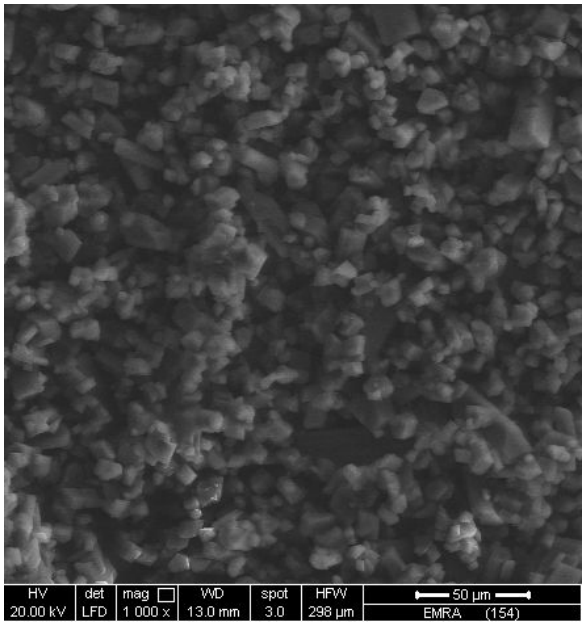

Figure 5A. SEM image of ZnO NPs synthesized by annealed zinc(II) glutaconate complex at 600 °C.

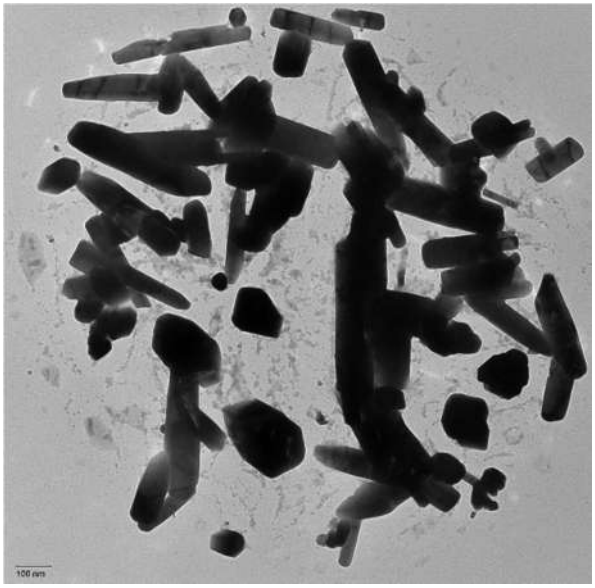

Figure 5B. TEM image of ZnO NPs synthesized by annealed zinc(II) glutaconate complex at 600 °C.

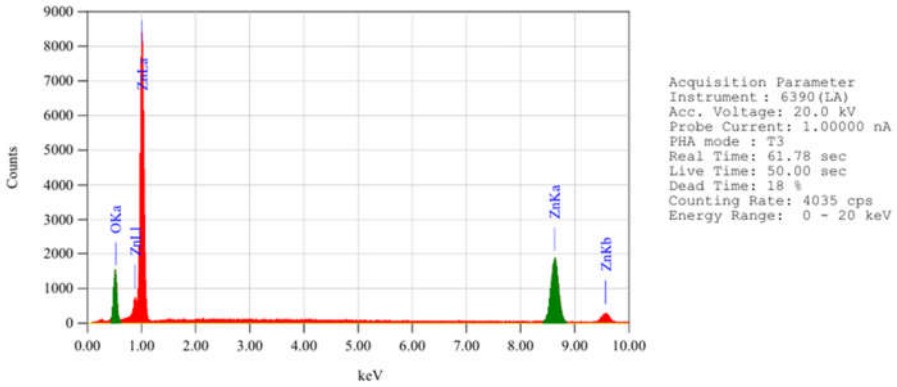

Figure 6. EDX spectrum of ZnO NPs which is synthesized by annealed zinc(II) glutaconate complex at 600 °C.

Catalytic activity of the ZnO NPs

The catalytic activity data for H_2O_2 degradation at room temperature and constant ZnO weight and H_2O_2 concentration (0.1 N) are listed in Table 3. The rate of H_2O_2 decomposition increased with time; the synthesized ZnO products from the thermal decomposition of zinc(II) glutaconate complex had a rate constant is 3.87×10^{-3} after 50 min [47]. Because the surface is very effective and has reactivable active areas, it may be used repeatedly to remove pollutants at a lower economic cost. It is also simple to create using readily available, low-cost components. One crucial stage in determining the practical utility of photocatalysts and creating heterogeneous photoactivity technologies for wastewater treatment is the regeneration of ZnO NPs. At a ZnO NPs catalyst weight of 100 mg, the catalytic impact of ZnO NPs on hydrogen peroxide breakdown demonstrates that the reaction rate of ZnO NPs is 3.87×10^{-3} $M^{-1}.min^{-1}$. Depending on the type of oxide, HO• has a different affinity for its surfaces. Inversely related to the variation in the metal cation's ionization potential is the trend for HO• adsorption energies onto the various metal oxides [30, 31].

Table 3. Catalytic activity data of the ZnO synthesized from the annealed zinc(II) glutaconate complex at 600 °C.

Results	t_{min}				
	10	20	30	40	50
$V_{(KMnO4)}$	5.6	5.4	5.2	5.1	5.0
$N_{(H2O2)}$ a–*x*	0.113	0.109	0.105	0.102	0.100
Ln(a–*x*)	-2.183	-2.219	-2.258	-2.284	-2.304
K	3.87×10^{-3}				

*K (min^{-1}) = rate constant of the H_2O_2 decomposition.

Photocatalytic degradation

The process of using photocatalysts to break down organic compounds that contaminate water or air or transform them into less hazardous chemicals has been shown to reduce the harm that organic color pollution does to both humans and the environment [39]. Consequently, the use of heterogeneous catalysts in photocatalysis research is intriguing as it aids in the complete mineralization of these environmentally dangerous dyes [40]. By varying the dosage of the appropriate synthetic materials and the duration of irradiation, the photodegradation of MB by synthetic nano zinc oxide was examined. The impact of various dosages of synthetic nano zinc oxide materials was investigated within the range of 50-600 mg in comparison to the MB dye solution. For the nanostructured zinc oxide, the photodegradation of dye was (~77%) at this dosage; beyond this optimal dosage, the dye's photodegradation was negligible. By setting the amount of ZnO NPs (50-600 mg) and varying the irradiation period from 20-240 min, the photodegradation of MB dye (%) was measured (Table 4). According to the aforementioned findings, the larger surface area of the nanostructured smart zinc oxide contributes to its higher photocatalytic efficiency. The low band gap energy of ZnO NPs (~3 eV) rather than that of the bulk ZnO, the ZnO NPs exhibits the highest photodegradation efficiency in the current investigation. The ZnO NPs has the lowest band gap energy and the highest photocatalytic efficiency. This could be because a lower band gap energy makes it easier to move an electron from valence band (VB) to conduction band (CB) and more holes are created in the VB, which in turn causes more ·OH radicals to be produced in the VB. In other words, the more electrons there are in the CB, the more superoxide radicals it will produce. According to earlier research in the literature, organic pollutants like MB dye photodegrade due to the action of $\cdot O_2^-$ and ·OH radicals [48].

Table 4. The relationship results between photodegradation of MB (%) against dosage of ZnO NPs (mg) and time of UV-irradiation (min).

Dosage ZnO NPs, mg	Photodegradation MB dye, %	Time UV-irradiation, min	Photodegradation MB dye, %
50	60	20	62
100	62	40	64
150	63	60	65
200	65	80	66
250	67	100	68
300	69	120	70
350	71	140	71
400	72	160	73
450	73	180	74
500	75	200	75
550	76	220	77
600	77	240	80

CONCLUSION

Zinc oxide nanoparticles with hexagonal structure is synthesized successfully with annealed zinc(II) glutaconate complex at 600 °C. Synthesized zinc oxide nanoparticles were characterized by FTIR, SEM, EDX, and XRD. From the TEM study, it is found that particles have with average size of ~50 nm. Global environmental contamination by coloured effluents is a serious concern, therefore, our study aims to evaluate the applicability of Zinc oxide nanoparticles, ZnO NPs for the removal of methylene blue (MB) from wastewater solution and also to study the catalytic

activity performance of the prepared ZnO NPs examined by the degradation of H_2O_2 solution. The highest dye removal rates associated with ZnO-NPs could be due to either the high production of reactive oxygen species (ROS), which are essential for dye degradation, or the large number of active sites on nano-catalyst surfaces that increase with concentration.

ACKNOWLEDGEMENT

This work was funded by the Deanship of Graduate Studies and Scientific Research at Jouf University under grant No. (DGSSR-2023-02-02259).

REFERENCES

1. Refat, M.S.; Saad, H.A.; Gobouri, A.A.; Alsawat, M.; Belgacem, K.; Majrashi, B.M.; Adam, A.M.A. Synthesis, characterization, and photocatalytic efficiency of a new smart PdO oxide nanomaterial for using in the recycling and sustainable wastewater treatment, *Bull. Chem. Soc. Ethiop.* **2021**, 35, 107-118.
2. Al-Hazmi, G.H.; Adam, A.M.A.; El-Desouky, M.G.; El-Bindary, A.A.; Alsuhaibani, A.M.; Refat, M.S. Efficient adsorption of rhodamine b using a composite of Fe3O4@ZIF-8: Synthesis, characterization, modeling analysis, statistical physics and mechanism of interaction, *Bull. Chem. Soc. Ethiop.* **2023**, 37, 211-229.
3. Segev-Bar, M.; Haick, H. Flexible sensors based on nanoparticles. *ACS Nano* **2013**, 7, 8366-8378.
4. Zhou, W.; Wachs, I.E.; Kiely, C.J. Nanostructural and chemical characterization of supported metal oxide catalysts by aberration corrected analytical electron microscopy. *Curr. Opin. Solid State Mater. Sci.* **2012**, 16, 10-22.
5. Pei, Z.; Xu, H.; Zhang, Y. Preparation of Cr_2O_3 nanoparticles via C_2H_5OH hydrothermal reduction, *J. Alloys Compd.* **2009**, 468, L5-L8.
6. El-Sheikh, S.M; Mohamed, R.M; Fouad, O.A. Synthesis and structure screening of nanostructured chromium oxide powders. *J. Alloys Compd*. **2009**, 482, 302-307.
7. Fu, X.Z.; Luo, X.X.; Luo, J.L.; Chuang, K.T.; Sanger, A.R.; Krzywicki, A. Ethane dehydrogenation over nano-Cr_2O_3 anode catalyst in proton ceramic fuel cell reactors to co-produce ethylene and electricity. *J. Power Sources* **2011**, 196, 1036-1041.
8. Kim, D.W.; Oh, S.G. Agglomeration of chromia nanoparticles prepared by amorphous complex method using chelating effect of citric acid. *Mater. Lett*. **2005**, 59, 976-980.
9. Li, L.; Yan, Z.; Lu, G.Q.; Zhu, Z.H. Synthesis and structure characterization of chromium oxide prepared by solid thermal decomposition reaction. *J. Phys. Chem. B* **2006**, 110, 178-183.
10. Abecassis-Wolfovich, M.; Rotter, H.; Landau, M.V.; Korin, E.; Erenburg, A.I.; Mogilyansky, D.; Gartstein, E. Texture and nanostructure of chromia aerogels prepared by urea-assisted homogeneous precipitation and low temperature super critical drying. *J. Non Cryst. Solids* **2003**, 318, 95-111.
11. Balchandran, U.; Siegel, R.W.; Liao, Y.X.; Askew, T.R. Synthesis, sintering and magnetic properties of nanophase Cr2O3. *Nanostruct. Mater.* **1995**, 5, 505-512.
12. Vollath, D.; Szabo, D.V.; Willis, J.O. Magnetic properties of nanocrystalline Cr_2O_3 synthesized in a microwave plasma. *Mater. Lett*. **1996**, 29, 271-279.
13. Singh, H.; Du, J.; Singh, P.; Yi, T.H. Ecofriendly synthesis of silver and gold nanoparticles by Euphrasia officinalis leaf extract and its biomedical applications. *Artif. Cells Nanomed. Biotechnol.* **2018**, 46, 1163-1170.
14. Furno, F.; Morley, K.S.; Wong, B.; Sharp, P.L; Arnold, P.L.; Reid, H.; silver nano particles and polymeric medical devices: A new approach to prevention of infection. *J. Antimicrob. Chemother.* **2004**, 54, 1019-1024.

15. Chorawalaa, K.K.; Mehali, M.J. Applications of nanotechnology in wastewater treatment. *Int. J. Innov. Emerg. Res. Eng.* **2015**, 2, 21-26.
16. Kumar, S.S.; Venkateswarlu, P.; Rao, V.R.; Rao, G.N. Synthesis, characterization and optical properties of zinc oxide nanoparticles. *Int. Nano Lett.* **2013**, 3, 1-6.
17. Velmurugan, R.; Swaminathan, M. An efficient nanostructured ZnO for dye sensitized degradation of Reactive Red 120 dye under solar light. *Sol. Energy Mater Sol. Cells* **2011**, 95, 942-950.
18. Wieghardt, K. The active sites in manganese-containing metalloproteins and inorganic model complexes. *Angew. Chem. Int. Ed. Engl.* **1989**, 28, 1153-1172.
19. Pecoraro, V.L.; Baldwin, M.J.; Gelasco, A. Interaction of manganese with dioxygen and its reduced derivatives. *Chem. Rev*. **1994**, 94, 807-826.
20. Rane, K.S.; Verenkar, V.M.S. Synthesis of ferrite grade γ-Fe_2O_3. *Bull. Mater. Sci*. **2001**, 24, 39-45.
21. Mehrotra, R.C.; Bohra, R. *Metal Carboxylates*, Academic Press: London; **1983**.
22. Mehrotra, R.C.; Singh, A.; Bhagat, M. Synthesis and characterization of heterozirconium chloride alkoxides containing bivalent main group metals. *Syn. React. Inorg. Matel-Org. Chem.* **1998**, 28,997-1011.
23. Srinivasan, B.R.; Sawant, S.C. Thermal and spectroscopic characterization of Mg(II) complexes of nitro-substituted benzoic acids. *Thermochim. Acta* **2003**, 402, 45-55.
24. Laws, EA. *Aquatic Pollution: An Introductory Text*. 3rd ed., John Wiley and Sons: New York; **2000**.
25. Duruibe, J.O.; Ogwuegbu, M.C.; Egwurugwu, J.N. Heavy metal pollution and human biotoxic effects. *Int. J. Phys. Sci.* **2007**, 2, 112-118.
26. Ramnani, P.; Saucedo, N.M.; Mulchandani, A. Carbon nano material–based electrochemical biosensors for label–free sensing of environmental pollutants. *Chemosphere* **2016**,143, 85-98.
27. Ingale, A.G.; Chaudhari, A.N. Biogenic synthesis of nanoparticles and potential applications: An eco-friendly approach. *JNMNT* **2013**, 4, 1-7.
28. Davis, M.E.; Chen, Z.; Shin, D.M. Nanoparticle therapeutics: An emerging treatment modality for cancer. *Nanosci. Technol.* **2009**, 7, 239-250.
29. Akinyemi, A.; Agboola, O.; Alagbe, E.; Igbokwe, E. The role of catalyst in the adsorption of dye: Homogeneous catalyst, heterogeneous catalyst, and advanced catalytic activated carbon, critical review. *Desalin. Water Treat.* **2024**, 320, 100789.
30. Li, Y.; Guo, H.; Li, H.; Wang, T. Performance of dye-containing wastewater treatment using Mn_xO_y-catalyzed persulfate oxidation. *Catal.* **2024**, 14, 758.
31. Chen, P.; Cheng, Z.; Zhang, X.; Zhang, L.; Zhang, X.; Tang, J.; Qiu, F. Efficient degradation of dye wastewater by catalytic ozonation reactive ceramic membrane with facile spraying of nano TiMn oxides: A pilot scale attempt. *JWPE* **2023**, 55, 104143.
32. Anandhi, G.; Iyapparaja, M. Photocatalytic degradation of drugs and dyes using a maching learning approach. *RSC Adv.* **2024**, 14, 9003-9019.
33. Pradhan, M.R.; Nanda, B.B.; Subhadarshini, A.; Panda, L.; Nanda, B. Enhanced catalytic reductive hydrogenation of an organic dye by Ag decorated graphitic carbon nitride modified MCM-41. *RSC Adv.* **2024**, 14, 1072-1081.
34. Liu, B.; Zhao, X.; Terashima, C.; Fujishima, A.; Nakata, K. Thermodynamic and kinetic analysis of heterogeneous photocatalysis for semiconductor systems. *Phys. Chem. Chem. Phys.* **2014**, 16, 8751-8760.
35. Sarmah, S.; Kumar, A. Photocatalytic activity of polyaniline-TiO_2 nanocomposites. *Indian J. Phys.* **2008**, 85, 713-726.
36. Alderman, D.J.; Clifton-Hadley, R.S. Malachite green: A pharmacokinetic study in rainbow trout, *Oncorhynchus mykiss* (Walbaum). *J Fish Dis*. **1993**, 16, 297-311.

37. Ramezani, S.; Pourbabaee, A.A.; Javaheri, J.A.; Bioremed, J. Photocatalytic performance of ZnO nanomaterials for self-sensitized degradation of malachite green dye under solar light. *Biodegrad.* **2013**, 4, 1000175.
38. Mittal, A. Adsorption kinetics of removal of a toxic dye, Malachite Green, from wastewater by using hen feathers. *J. Hazard. Mater*. **2006**, 133, 196-202.
39. Liu, Y.; Ohko, Y.; Zhang, R.; Yang, Y.; Zhang, Z. Degradation of malachite green on Pd/WO_3 photocatalysts under simulated solar light. *J. Hazard. Mater.* **2010**, 184, 386-391.
40. Prado, A.G.; Costa, L.L. Photocatalytic decouloration of malachite green dye by application of TiO_2 nanotubes. *J. Hazard. Mater.* **2009**, 169, 297-301.
41. Refat, M.S. Synthesis and characterization of ligational behavior of curcumin drug towards some transition metal ions: Chelation effect on their thermal stability and biological activity. *Spectrochim. Acta Part A* **2013**, 105, 326-337.
42. Nakamoto, K. *Infrared and Raman Spectra of Inorganic and Coordination Compounds*, Wiley: New York; **1997**.
43. Patil, A.V.; Dighavkar, C.G.; Sonawane, S.K.; Borse, R.Y. Effect of firing temperature on structural parameters of screen printed ZnO thick films. *Invertis. J. Sci. Technol.* **2010**, 3, 207-214.
44. Arora, A.K.; Devi, S.; Jaswal, V.S.; Singh, J.; Kinger, M.; Gupta, V.D. Synthesis and characterization of ZnO nanoparticles. *Orient. J. Chem*. **2014**, 30, 1671-1679.
45. Cullity, B.D.; *Elements of X-Ray Diffraction*, Addison-Wesley: Reading, MA; **1972**, p. 102.
46. Rawashdeh, R.Y.; Harb, A.M.; AlHasan, A.M. Biological interaction levels of zinc oxide nanoparticles; lettuce seeds as case study. *Heliyon* **2020**, 6, 1-10.
47. Zigah, D.; Lopez, J.R.; Bard. A. Quantification of photoelectrogenerated hydroxyl radical on TiO_2 by surface interrogation scanning electrochemical microscopy. *J. Phys. Chem*. **2012**, 14, 12764-12772.
48. Shi, C.; Nie, Z.H.; Zhao, L.; Lu, L.; Cheng, F.; Chen, X.; Tan, G.; Liu, Q.Q.; Wang, J.; Chauhan, R.; Kumar, A. Efficient degradation of dyes in water by two Ag-based coordination polymers containing 1,3-bis(3,5-dicarboxylphenoxy)benzene and N-donor linkers. *Polyhedron* **2021**, 207, 115362-115369.